

http://pubs.acs.org/journal/aesccq Article

High-Temperature Inter-Mineral Potassium Isotope Fractionation: Implications for K-Ca-Ar Chronology

W. Wilson Kuhnel, Stein B. Jacobsen, Yonghui Li, Yaray Ku, Michail I. Petaev, Shichun Huang, Zhongqing Wu, and Kun Wang*



Cite This: ACS Earth Space Chem. 2021, 5, 2740–2754



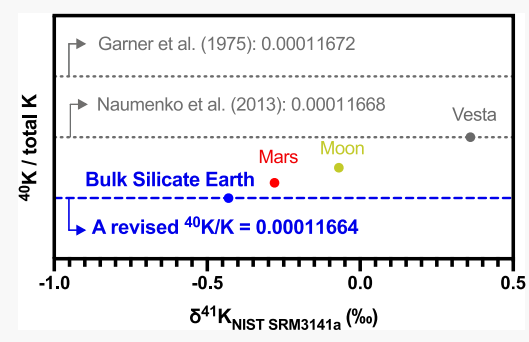
ACCESS

III Metrics & More

Article Recommendations

s Supporting Information

ABSTRACT: Recent advances in high-precision potassium (K) isotopic analysis have found considerable isotopic variation in rock samples of the Earth's continental and oceanic crusts; however, it is still uncertain whether there is any resolvable inter-mineral and mineral-melt K isotopic fractionation during igneous and metamorphic processes. Here, we report K isotope compositions of mineral separates from three extremely well-preserved igneous rocks (intrusive/extrusive and mafic/intermediate/felsic) in order to investigate possible inter-mineral and mineral-melt K isotopic fractionation at magmatic temperatures. For the first time, we found large inter-mineral fractionation of K isotopes in natural samples (up to 1.072%), where plagioclase displays a significant enrichment of heavier K isotopes compared to potassium feldspar and biotite in granite. In addition, we also observed smaller but measurable K



isotope fractionation (0.280 ± 0.030%) between ternary feldspar phenocrysts and matrices in a trachyandesite, as well as a comparable isotope fractionation $(0.331 \pm 0.010\%)$ between plagioclase and the bulk in a gabbroic intrusive rock. We also evaluated such results by comparing the theoretically calculated equilibrium K isotope fractionation factors between relevant igneous minerals in the literature and this study. In general, the measured inter-mineral fractionations are consistent with the theoretical calculations (i.e., plagioclase is enriched in heavier isotopes compared to potassium feldspar). Specifically, the measured K isotope fractionation between the phenocryst rim and matrix in the trachyandesite agrees well with the calculated equilibrium isotope fractionation. However, the measured K isotope fractionations between the phenocryst core and matrix as well as between plagioclase and K-feldspar are significantly larger (by a factor of $\sim 2-3$) than the calculated isotope fractionations, which suggest isotopic disequilibrium due to kinetic processes. Using a range of plagioclase-melt isotope fractionation factors inferred from the theoretical calculations in this study, we modeled the K isotopic fractionation during the formation of lunar anorthositic crust, and the result shows a negligible effect on the K isotopic compositions in both lunar crust and mantle. The K isotopic difference between the Earth and the Moon, therefore, cannot be the result of lunar magma ocean differentiation. Finally, we evaluate the effect of observed inter-mineral fractionations on K-Ar and 40Ar-39Ar dating. This study indicates that the variation of the 40K/K ratio would contribute a maximum 0.08% error to the K-Ar and 40Ar-39Ar age uncertainties. We propose a refined 40K/total K ratio as $0.00011664 \pm 0.00000011$ (116.64 ± 0.11 ppm) instead of the conventional value, 0.0001167(2), for the present Earth. Because some minerals fractionate K isotopes, ultrahigh-precision age dating with the K-Ca-Ar dating systems must measure the K isotope fractionation in the same mineral fractions used for age dating.

KEYWORDS: potassium isotopes, MC-ICP-MS, inter-mineral fractionation, K-Ar dating, Ar-Ar dating

1. INTRODUCTION

Potassium (K) is one of the most abundant elements in the Earth's crust. Potassium occurs naturally as three isotopes: ³⁹K (93.26%), ⁴⁰K (0.0117%), and ⁴¹K (6.73%). Potassium-40, the radioactive parent to both ⁴⁰Ca (89.5%) and ⁴⁰Ar (10.5%), has a half-life of 1.248 billion years and forms the basis for the K—Ca, K—Ar, and Ar—Ar dating systems. The high-precision measurements of K isotopes can be traced back to the 1990s, when an extensive survey of geological samples by Humayun and Clayton found no measurable K isotopic difference on Earth. However, with the development of multiple-collector inductively coupled-plasma mass-spectrometry (MC-ICP-MS), the

measurements of K isotopes have been significantly improved, and considerable isotopic variations of K have been observed in bulk igneous and sedimentary rocks, clay, evaporite minerals, and seawater samples.^{4–13} The K isotopic variations observed on Earth have been mostly attributed to low-temperature

Received: May 19, 2021 Revised: September 28, 2021 Accepted: September 30, 2021 Published: October 12, 2021





geochemical processes such as continental weathering, hydrothermal alteration, and authigenic clay formation. 6,14-22 However, it is still unknown whether there is any significant inter-mineral K isotope fractionation during high-temperature igneous processes. Any inter-mineral fractionation of K isotopes is important for the accuracy of K–Ca–Ar dating because current calculations assume a constant ⁴⁰K abundance across different samples and minerals (cf. Morgan et al., ²³), with the ⁴⁰K/K ratio being equal to 0.0001167(2), as measured in the NIST standard SRM985. ²⁴ This assumption needs to be revisited because large K isotopic variations have been observed in terrestrial rocks.

In order to examine possible inter-mineral K isotopic fractionation in igneous rocks and to estimate the fractionation factors under relevant crustal magmatic temperatures, we analyzed bulk samples and K-rich mineral separates from one granite, one trachyandesite, and one gabbro. We compare these data with the theoretical calculations of equilibrium K isotopic fractionation factors to provide an independent evaluation on the validity of those ab initio calculations. We will assess the potential implications of inter-mineral K isotopic fractionation for the formation of lunar anorthositic crust, as well as for the K—Ca—Ar chronology, and provide a refined 40 K/K ratio which better suits igneous systems.

2. SAMPLES AND METHODS

2.1. Sample Description. For this study, we selected three extremely fresh and well-preserved igneous rocks (intrusive/extrusive and mafic/intermediate/felsic) for mineral separations. All rocks are from the Permian Oslo Rift in Norway, a part of the Skagerrak-Centered Large Igneous Province. The first is a biotite granite from the city of Drammen, the second is a trachyandesite (local name: rhomb porphyry) from Hole, a municipality in Viken county, near the city of Oslo, and the third is a gabbro from Dignes in Modum, a municipality in Viken county. These unaltered samples are excellent for investigating K isotope fractionation between some common igneous minerals with significance to high K concentrations.

Granite OGD-1 was sampled from the Drammen batholith (650 km²), the largest granite complex within the mainly alkaline province of the Permo-Carboniferous Oslo Rift.²⁵ It is a peraluminous granite with both perthitic alkali feldspars and plagioclase.

The trachyandesite K1714 was sampled from the second lava flow (called RP_1) in the Krokskogen lava plateau of the Permian Oslo Rift. This flow, about 100 m thick, once covered most of the Oslo Rift. It contains large (cm-sized)-zoned feldspars embedded in a fine-grained matrix. Sm–Nd and Rb–Sr systematics reveal that it has Nd and Sr isotopic compositions similar to mantle-derived alkali basalts from oceanic islands (Jacobsen and Wasserburg²⁶).

The Dignes gabbro CP5.5 sample is one of the small Permian gabbroic intrusions surrounded by lower Paleozoic sediments and Precambrian basement in the Oslo rift, South Norway. This gabbro contains large (\sim 5 mm) crystals of subhedral plagioclase, which could be easily separated. The gabbro Rb–Sr age is \sim 266 Ma.²⁷

2.2. Sample Preparation and Chemical Purification of Potassium. The rock samples were first cut into thin (\sim 2-3 mm) slabs (Figure 1) and further crushed with a hand hammer wrapped with cleanroom wipes. Three potassium-bearing minerals—potassium feldspar, biotite, and plagioclase (Figure 1)—were handpicked from the crushed granite sample under a

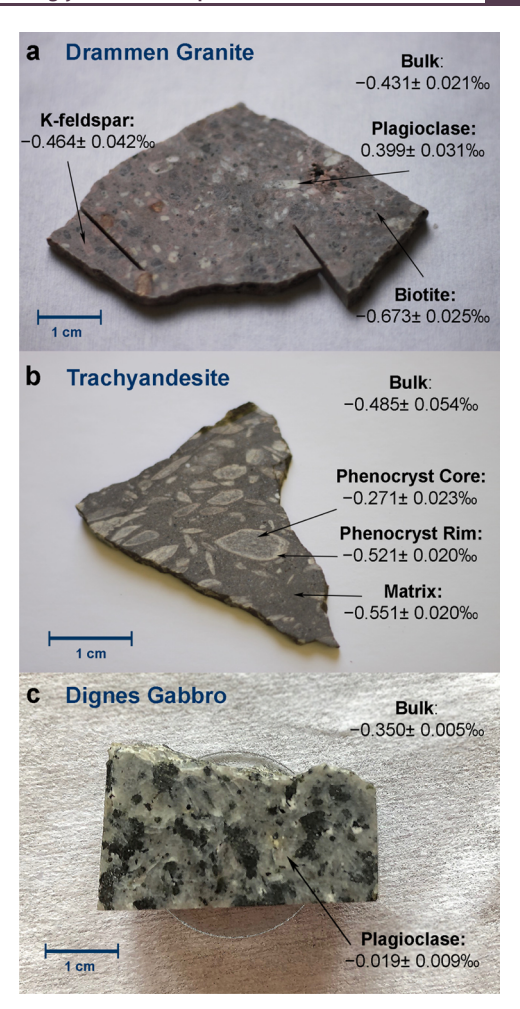


Figure 1. Photographs of the sample slabs labeled with K isotopic compositions ($\delta^{41}K_{SRM3141a}$) in each component. (a) Drammen granite. (b) Trachyandesite. (c) Dignes gabbro.

binocular microscope. For the trachyandesite, four samples were collected, consisting of the phenocryst core, the phenocryst rim, the matrix, and the bulk rock (Figure 1). For the gabbro, we selected only plagioclase and the bulk sample (Figure 1). Sample masses ranged from 9.5 to 99.6 mg (Table 1), which are enough for high-precision K isotope analyses given the relatively high concentration of K in each of these minerals.

All samples were digested with a CEM MARS 6 microwave digestion system. The samples were finely powdered using a mortar and pestle. They were then dissolved with an acid mixture consisting of concentrated 0.5 mL HF, 2 mL of HNO3, and 1 mL of HCl, then dried with heat lamps in an ultrapure nitrogen environment to remove SiF4. They were then dissolved again using a second mixture of diluted aqua regia consisting of 0.5 mL of concentrated HNO3, 1.5 mL of concentrated HCl, and 1 mL of $\rm H_2O$. The microwave digestion system was set at 400 W to reach a temperature of 230 °C (20 min ramping time + 60 min holding time + 30 min cooling time). Acid-washed Teflon beakers were used in all procedures.

We followed the potassium separation method detailed in the literature⁷ and based on methods first established by Strelow et al.²⁸ and subsequently used by Humayun and Clayton.³ Fully digested samples were loaded onto the 13 mL Bio-Rad AG50W-X8 cation exchange resin (100–200 mesh) chromatography

Table 1. Major Element Oxide Compositions (in wt %) of Bulk Samples and "Minerals" Analyzed with iCapQ ICP-MS

	granite				trachyandesite				gabbro	
	bulk	"plagioclase" ^a	"K-feldspar" ^a	"biotite" ^a	bulk	phenocryst core	phenocryst rim	matrix	bulk	"plagioclase" ^a
mass (mg)	19.2	19.2	22.7	9.5		21.7	11.5	16.6	99.6	49.0
percentage (wt %) ^a		18.05	62.83	2.42		6.06	1.11	70.92		
SiO ₂ ^b										
TiO_2	0.27	0.06	0.07	3.98	1.42	0.40	0.24	2.37	2.23	0.07
Al_2O_3	20.09	27.68	23.34	15.60	18.58	29.87	22.73	20.17	19.59	13.44
Cr_2O_3	0.00	0.00	0.00	0.00	0.00	0.00	0.00	0.00	0.00	0.00
FeO	1.04	0.68	0.58	17.92	5.46	1.68	0.77	7.77	9.93	0.15
MnO	0.03	0.01	0.01	0.61	0.14	0.05	0.04	0.19	0.16	0.00
MgO	0.37	0.08	0.04	17.36	1.40	0.34	0.46	1.87	3.62	0.02
CaO	0.69	3.35	0.36	2.79	4.53	8.66	5.53	5.72	7.82	4.76
Na ₂ O	0.67	3.22	0.35	2.69	4.36	8.34	5.33	5.51	4.94	3.28
K_2O	7.29	1.57	11.03	7.34	4.65	3.54	2.20	5.30	1.6	0.82
P_2O_5	0.05	0.02	0.01	0.70	0.64	0.12	0.23	1.28	0.36	0.08
Or (mol %)		16.9	93.0			15.1	14.7	28.7		8.4
Ab (mol %)		52.8	4.5			54.0	54.2	45.3		50.8
An (mol %)		30.3	2.5			31.0	31.1	26.0		40.8

"All "minerals" are crushed and handpicked, which are not pure and have other mineral fragments attached to them. "SiO₂ was not measured because Si was lost during HF digestion.

Table 2. Average Major Element Oxide Compositions (in wt %) of Minerals Analyzed with an Electron Microprobe^a

		gra	nite	trachyandesite				
	plagioclase	1SD	K-feldspar	1SD	phenocryst	1SD	matrix	1SD
SiO ₂	67.25	0.85	65.68	0.84	62.30	1.72	65.71	0.90
TiO_2	0.02	0.04	0.02	0.02	0.13	0.11	0.11	0.16
Al_2O_3	20.14	0.59	18.81	0.51	23.23	1.50	19.24	0.74
Cr_2O_3	0.02	0.03	0.02	0.03	0.02	0.03	0.02	0.03
FeO	0.16	0.17	0.18	0.13	0.46	0.19	0.52	0.33
MnO	0.03	0.05	0.02	0.03	0.03	0.05	0.04	0.05
MgO	0.04	0.05	0.00	0.01	0.18	0.17	0.26	0.28
CaO	0.40	0.45	0.13	0.22	2.91	1.56	0.62	0.39
Na ₂ O	11.20	1.18	3.80	2.93	8.30	1.44	6.85	2.57
K_2O	0.75	1.52	11.33	4.16	2.45	1.87	6.63	3.74
Or (mol %)	4.1		65.8		14.0		37.8	
Ab (mol %)	94.0		33.6		72.1		59.3	
An (mol %)	1.8		0.7		13.9		3.0	

^aSee the Supporting Information for individual measurement.

columns in 0.5 N HNO_3 . Potassium is eluted out of the solution between 180 and 340 mL of 0.5 N HNO_3 .

The eluted K cuts were first analyzed with a Thermo Scientific iCAP QICP-MS to determine whether potassium accounted for >99% of the dissolved cations in the sample solutions to exclude a possible matrix effect. Titanium (Ti) was detected in one sample (granite biotite) at levels of $\sim\!8\%$ relative to K in the solution. After a second pass using a smaller column (1.6 mL Bio-Rad AG50W-X8 cation exchange resin), potassium made up more than 99% of the cations in the sample solutions.

2.3. Elemental Analysis by ICP-MS and Electron Microprobes. An aliquot of each fully dissolved sample (prior to the column purification procedure) was analyzed with a Thermo Scientific iCAP Q ICP-MS for major elements. The sample solutions were introduced into the plasma with a Peltier cooled cyclonic spray chamber and a Teflon PFA nebulizer. The single collision cell mode with kinetic energy discrimination was used in analysis. Pure He was introduced as the collision gas. Blank solutions and 1:5000 solutions (in 2% nitric acid) of USGS standards BHVO-1, AGV-1, BCR-1 yielded

excellent linear calibration curves. Typical precisions are a few % RSD for major elements. The results are shown in Table 1.

Slices of the granite and trachyandesite were polished for electron microprobe analysis. Chemical compositions of minerals were determined by a JEOL Super Probe 733 equipped with automation software by Geller Microanalytical using 15 kV accelerating voltage, 20 nA beam current, and peak counting times of 40 s. Natural and synthetic minerals were used as elemental standards. All analyses were corrected using the Armstrong—Bence—Albee correction procedure built in the automation software package. The average mineral compositions are reported in Table 2, while the individual analyses are reported in the Supporting Information (Table S1).

2.4. Potassium Isotope Analysis. The isotopic ratios of K were analyzed with either a GV Instruments IsoProbe P (for OGD-1 and K1714) or a Nu Instruments Sapphire (for CP5.5) MC-ICP-MS, both equipped with hexapole gas collision cells to remove argide-based (ArH⁺) interferences. High-precision K isotopic analysis has been routinely conducted at Harvard University since 2016, and the methods have been previously described and evaluated in detail.^{7,29} Sample solutions were

Table 3. Potassium Isotopic Compositions of Minerals and Bulk Rock Samples

	description	location	$\delta^{41} ext{K}_{ ext{Suprapur}} \left(\%_o ight)$	$\delta^{41} \mathrm{K_{SRM3141a}} \ (\%_0)^a$		2SE	n
granite		Drammen, Oslo Rift, Norway					
	plagioclase		0.446	0.399	±	0.031	29
	K-feldspar		-0.417	-0.464	±	0.042	34
	biotite		-0.626	-0.673	±	0.025	30
	bulk		-0.384	-0.431	±	0.021	32
			$\Delta^{41}K[Pl - Kfs] =$	0.863	±	0.052	
			$\Delta^{41}K[Kfs - Bt] =$	0.209	±	0.049	
			$\Delta^{41}K[Pl - Bt] =$	1.072	±	0.040	
trachyandesite		Krokskogen, Oslo Rift, Norway					
	phenocryst core		-0.224	-0.271	±	0.023	28
	phenocryst rim		-0.474	-0.521	±	0.020	18
	matrix		-0.504	-0.551	±	0.020	27
	bulk		-0.438	-0.485	±	0.054	10
			Δ^{41} K[core – matrix] =	0.280	±	0.030	
			Δ^{41} K[core - rim] =	0.250	±	0.030	
			Δ^{41} K[rim - matrix] =	0.030	±	0.028	
gabbro		Dignes, Oslo Rift, Norway					
	plagioclase		0.028	-0.019	±	0.009	17
	bulk		-0.303	-0.350	±	0.005	20
			Δ^{41} K[Pl - bulk] =	0.331	±	0.010	
NIST-SRM985 ^b			-0.330	-0.377	±	0.099	

^aThe data were converted from δ^{41} K_{Suprapur} to δ^{41} K_{SRM3141a} through the 0.047% difference between Suprapur and NIST-SRM3141a measured by Ku and Jacobsen. ²⁹ ^bThe δ^{41} K value for SRM985 relative to SRM3141a was obtained using the 0.259% difference between SRM985 and seawater measured by Morgan et al. ⁴ and the 0.118% difference between seawater and SRM3141a measured by Wang et al. ³⁴

introduced into the plasma source using a 100 μ L/min PFA MicroFlow nebulizer via an APEX-IR and ACM desolvation system for the Isoprobe P and APEX Omega for the Nu Sapphire. The K isotopic compositions are reported with conventional delta notation, where δ^{41} K = ([(^{41}K/^{39}K)_{sample}/(^{41}K/^{39}K)_{standard} - 1] × 1000). The fractionation between two minerals, A and B, is simply expressed as Δ^{41} K[A-B] = δ^{41} K[A] – δ^{41} K[B]. The K isotopic compositions of bulk samples and hand-picked non-pure "minerals" are reported in Table 3.

Our laboratory in-house bracketing standard is the Suprapur 99.995% purity potassium nitrate (KNO₃) purchased from Merck KGaA in 2014. In order to compare data with other laboratories, we report data relative to the NIST-SRM3141a value, where $\delta^{41} K_{SRM3141a} = \delta^{41} K_{Suprapur} - 0.047\%c.^{29}$ To eliminate any confusion, unless specified otherwise, all K isotope values mentioned below will be in $\delta^{41} K_{SRM3141a}$ notation.

2.5. Ab initio Calculations. Previously, Li et al. 30,31 calculated the reduced partition function ratios $(10^3 \ln \beta)$ for a series of K-bearing minerals including alkali feldspars (i.e., the solid solution of microcline and albite). In order to expand the database and to better fit to the case of anorthite (Section 4.2), we calculated the reduced partition function ratios for anorthite $(An_{15/16}Or_{1/16} \text{ and } An_{31/32}Or_{1/32})$ using Quantum ESPRESSO, which is based on the density functional theory (DFT) and plane wave basis set. The calculation details and the pseudopotentials used in this paper are the same as our published method papers, 30,31 where the beta values $(10^3 \ln \beta)$ for a full range of feldspar compositions have been reported as a function of temperature. Here, we only focus on the feldspar compositions relevant to this study. Please refer to our method papers 30,31 for computation details.

3. RESULTS

3.1. Elemental Composition. The major element compositions of bulk samples and hand-picked minerals (see

Figure 1) analyzed with the ICP-MS are reported in Table 1. These analyses were conducted on the aliquots from the same sample digestions that were used for K isotopic analysis. In addition, we also analyzed the mineral compositions in situ (using the electron microprobe) from the same hand samples of the granite and trachyandesite. The average mineral compositions analyzed with electron microprobe are reported in Table 2, and the individual analyses are listed in the Supporting Information The plagioclase compositions of the individual electron microprobe measurements are plotted in the An-Ab-Or ternary diagram (Figure 2). The compositions of the handpicked plagioclase and potassium feldspar analyzed with ICP-MS overlap with that measured by an electron microprobe. The small discrepancy (e.g., in Ca, Al, and Fe) can be attributed to the non-perfect separation; however, this discrepancy would not affect the K concentrations and isotopic compositions. The elemental compositions obtained for the trachyandesite's phenocryst and matrix using either the ICP-MS or the electron microprobe also agree well with each other, and both show that the trachyandesite's phenocryst and matrix are composed primarily of plagioclase feldspars. The plagioclase compositions vary from the phenocryst core (An₃₁Ab₅₄Or₁₅) and rim $(An_{31}Ab_{54}Or_{15})$ to the matrix $(An_{26}Ab_{45}Or_{29})$.

3.2. Potassium Isotope Composition. 3.2.1. Drammen Granite. The bulk K isotopic composition of the Drammen granite is $-0.431 \pm 0.021\%$, which is similar to other granites (e.g., USGS reference material G2 from Bradford, Rhode Island)^{5,10,32} and is not significantly different from the Bulk Silicate Earth (BSE) value $(-0.43 \pm 0.17\%)$. The K isotopic composition of potassium feldspar $(-0.464 \pm 0.042\%)$ does not differ substantially from the bulk, consistent with the fact that potassium feldspar is the major host mineral of K in granite. Biotite is enriched in lighter K isotopes $(-0.673 \pm 0.025\%)$ relative to the bulk. Plagioclase is enriched in heavier K isotopes of $+0.399 \pm 0.031\%$. This is the first detection of a large (>1%)

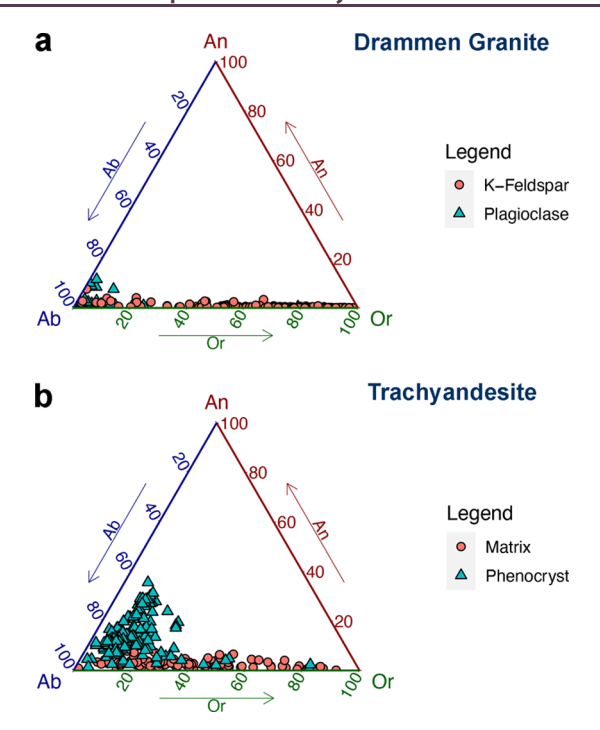


Figure 2. Feldspar ternary diagrams displaying all individual electron microprobe data for plagioclase and K-feldspar in Drammen granite (a) and in the trachyandesite (b).

inter-mineral K isotope fractionation in an igneous system except for pegmatites.⁴

3.2.2. Krokskogen Trachyandesite (Rhomb Porphyry— RP_1). The bulk composition of the trachyandesite is $-0.485 \pm 0.054\%e$, which is indistinguishable from the BSE value ($-0.43 \pm 0.17\%e$). The phenocrysts ($An_{31}Ab_{54}Or_{15}$ for both cores and rims) and matrix ($An_{26}Ab_{45}Or_{29}$) contain similar amounts of An and Ab end members but differ significantly in Or. The phenocryst core displays a significantly higher value ($-0.271 \pm 0.023\%e$) than the bulk. The phenocryst rims and matrix have similar K isotopic compositions ($-0.521 \pm 0.020\%e$ vs $-0.551 \pm 0.020\%e$) indistinguishable from the bulk rock within the uncertainty.

3.2.3. Dignes Gabbro. The bulk composition of the gabbro is $-0.350\pm0.005\%$, which is significantly higher than the BSE value $(-0.43\pm0.17\%)$. 33 The hand-picked plagioclase feldspar $(An_{41}Ab_{51}Or_8)$ shows an even higher value $(-0.019\pm0.009\%)$ compared to the bulk and BSE values. K-poor plagioclase feldspars are consistently enriched in heavy K isotopes compared to K-rich plagioclase and potassium feldspars. This is observed in all three igneous rock systems in this study and is consistent with the prediction from theoretical calculations. 30

3.2.4. Evaluation of Data Validity According to Mineral Modal Percentage. To check the internal consistency and verify whether the reconstructed K isotopic values of the bulk granite and trachyandesite agree with the measured values of bulk samples, we used the elemental compositions (Table 1) to solve for each mineral's percentage in the bulk samples. The best fit for the granite is 18.05 wt % of plagioclase, 62.83 wt % of potassium feldspar, and 2.42 wt % of biotite. The best fit for the trachyandesite is 6.06 wt % of the phenocryst core, 1.11 wt % of the phenocryst rim, and 70.92 wt % of the matrix. We applied those mineral modal percentages to reconstruct the bulk values using the following equation

$$\frac{\sum \text{bulk \%}_{\text{mineral}} \times \delta^{41/39} K_{\text{mineral}} \times \text{wt \% } K_2 O_{\text{mineral}}}{\sum \text{bulk \%}_{\text{mineral}} \times \text{wt \% } K_2 O_{\text{mineral}}}$$
(1)

The reconstructed bulk for granite is $-0.436 \pm 0.041\%$, which matches well with the measured bulk value $(-0.431 \pm 0.021\%$). Similarly, the reconstructed bulk for the trachyandesite of $-0.536 \pm 0.020\%$ is within the uncertainty of the measured bulk value $(-0.485 \pm 0.054\%)$. The agreements between reconstructed and measured bulks lend confidence to the validity of the observed inter-mineral fractionations in this study.

3.3. K–O Bond Lengths and Reduced Partition Function Ratios in Anorthite. We have previously calculated the K–O bond lengths and reduced partition function ratios for alkali feldspars (from $\mathrm{Ab_{15/16}Or_{1/16}}$ to $\mathrm{Ab_{0/16}Or_{16/16}})^{30,31}$ Using the same methods, we calculated the K–O bond lengths and reduced partition function ratios (10^3 ln β) for anorthite ($\mathrm{An_{15/16}Or_{1/16}}$ and $\mathrm{An_{31/32}Or_{1/32}}$) in order to better fit to the case of lunar anorthite discussed in this study (Section 4.2). The average K–O bond lengths for $\mathrm{An_{15/16}Or_{1/16}}$ and $\mathrm{An_{31/32}Or_{1/32}}$ are illustrated in Figure 3. Compared to alkali feldspar (e.g.,

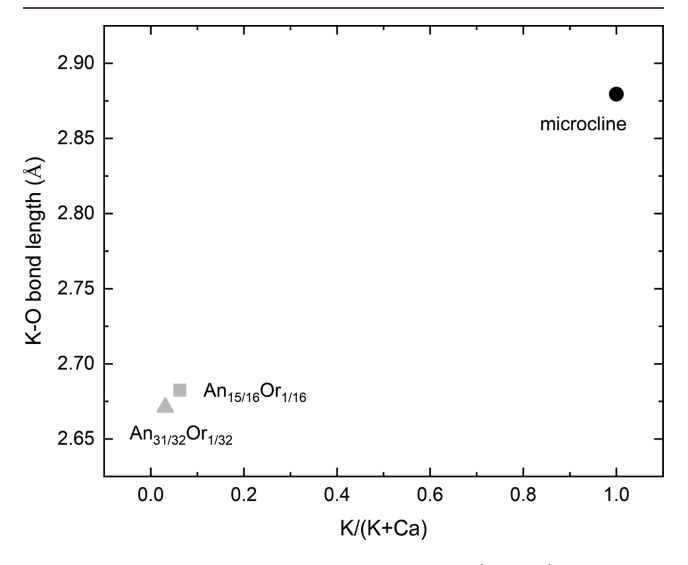


Figure 3. Average nearest K–O bond length vs K/(K + Ca) of feldspars (microcline, $An_{15/16}Or_{1/16}$, and $An_{31/32}Or_{1/32}$). K/(K + Ca) = 1, 1/16, or 1/32. Microcline are from the literature 30,31 and anorthite from this study.

Ab_{15/16}Or_{1/16}), the K–O bond length of anorthite (e.g., An_{15/16}Or_{1/16}) is significantly shorter (2.68 Å vs 2.72 Å), 30,31 thus preferentially enriched in heavier K isotopes. The An_{31/32}Or_{1/32} has the shortest K–O bond length and the largest K isotopic fractionation compared to the microcline (see Figures 3 and 4A).

4. DISCUSSION

4.1. High-Temperature Potassium Isotopic Fractionation between Minerals. In recent years, with the advances in MC-ICP-MS, it is now possible, for the first time, to resolve the K isotopic differences between different types of samples, particularly between high-temperature igneous and low-temperature sedimentary rocks, clay and evaporite minerals, and riverand sea-water samples. However, little K isotopic fractionation has been found among bulk igneous rocks, as shown by a suite of igneous rocks (from basalts to rhyolites)

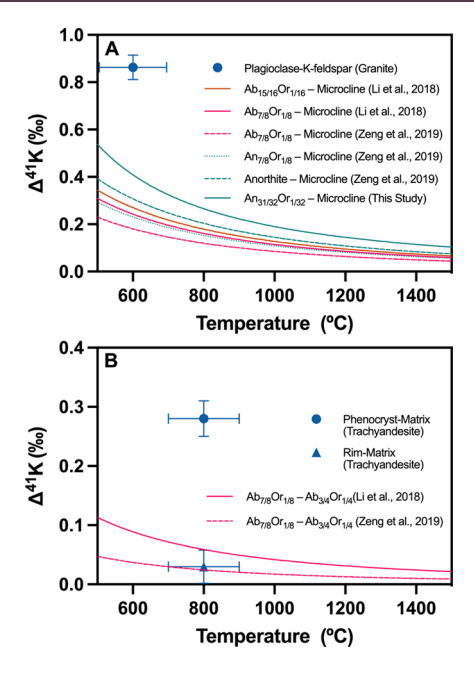


Figure 4. Inter-mineral potassium isotope compositions in granite (A) and trachyandesite (B) measured in this study vs temperature. The ab initio calculations for K isotope equilibrium fractionation factors between K-bearing minerals at temperature varying from 500 to 1500 $^{\circ}\text{C}$ are also shown. 30,31,38 The temperatures for granite (600 $^{\circ}\text{C}$) and trachyandesite (800 $^{\circ}\text{C}$) are arbitrarily selected in order to compare with ab initio calculations. Note that most of the measured intermineral potassium isotope compositions are significantly larger than the calculated fractionations at any reasonable magmatic temperature, except for the fractionation between the phenocryst rim and matrix in the trachyandesite.

from a single volcano system, ³⁶ as well as by a global database of fresh oceanic basalt samples. ³³ This is consistent with the fact that K is an incompatible element, and it preferentially enters the melt during partial melting. In addition, according to the "rule-of-thumb" of isotope fractionation, ³⁷ the equilibrium isotope fractionation approaches zero with increasing temperatures, hinting at no fractionation between minerals at high temperatures. Thus, K isotopes tend not to fractionate during magmatic differentiation (e.g., partial melting and fractional crystallization). Except for the minerals separated from pegmatites and one tuff, ⁴ no K isotopic fractionation has been reported for igneous minerals. The large fractionation (up to 1.250%o) among minerals separated from pegmatites (e.g., lepidolite, muscovite, amazonite, astrophyllite, potassium feldspar, polylithionite, and biotite) has been attributed to the fluid—rock interaction. ⁴

However, in this study, we observed large (up to $1.072 \pm 0.040\%$) isotopic fractionations between minerals in all three different igneous rocks (whether intrusive/extrusive or mafic/intermediate/felsic) that are well-resolvable with the current analytical uncertainty. Particularly, the plagioclase is consistently enriched in heavier K isotopes compared to the potassium feldspar, other K-bearing minerals (e.g., biotite), and the bulk. Plagioclases with lower K concentrations also have higher isotopic values than plagioclases with higher K concentrations. These observations are overall consistent with theoretical calculations of the equilibrium fractionation factors of K isotopes among common K-bearing minerals.

First-principle calculations based on DFT have recently been applied to the K isotope system, and the reduced partition

function ratios $(10^3 \ln \beta)$ for a series of K-bearing minerals have been calculated. ^{30,31,38,39} At any specific temperature, the intermineral equilibrium isotope fractionation factor (Δ^{41} K_{a-b} = 10^3 $\ln \beta_a - 10^3 \ln \beta_b$) is determined by their relative bond strengths. The heavier isotopes are preferentially enriched in the minerals with stronger bonds. The bond strength, in turn, is a function of the bond length, coordination number, ionic charge, and the bonded anions.³⁷ When other conditions are equal, the shorter bond is stronger than the longer bond. Li et al.30 investigated the K concentration effects on K-O bond lengths and the resulting K isotopic effects in alkali feldspars. They found that the higher the K concentration, the longer the K-O bond (weaker bond strength). Microcline (K/(K + Na +Ca) = 1) has the longest average K-O bond (2.88 Å), while plagioclase with lower K concentrations (K/(K + Na + Ca) < 1)has a shorter bond (~2.65 Å) (Figure 3). Hence, low-K plagioclases have stronger bond strengths and are enriched in heavier K isotopes.³⁰ This prediction is consistent with what we have observed in all three igneous rocks, where low-K plagioclases show higher K isotopic values than high-K plagioclases and potassium feldspars (Figure 4).

Although our observations of inter-mineral isotope fractionations in natural samples generally agree with the theoretical calculations in the direction of fractionation, the magnitudes of fractionation do not always match. As shown in Figure 4, we plotted the measured fractionations between the plagioclase and potassium feldspar in granite and between the phenocryst core/ rim and matrix in the trachyandesite versus temperatures. The three pairs studied here are compared to the theoretically calculated inter-mineral equilibrium isotope fractionation factors between low-K plagioclase and microcline. 30,31 Only the isotope fractionation between the phenocryst rim and matrix in the trachyandesite matches well with the calculated intermineral equilibrium isotope fractionation factor (see Figure 4B). The measured fractionation between the phenocryst core and the matrix in the trachyandesite and that between plagioclase and K-feldspar in granite are larger by a factor of $\sim 2-3$ (see Figure 4A). For example, at 600 °C, ab initio calculation indicates a 0.41% fractionation between low-K plagioclase (e.g., K/(K + Na + Ca) = 1/32) and microcline, but the measured fractionation between plagioclase and potassium feldspar of $0.863 \pm 0.052\%$ is about 2× larger. As shown in Figure 4, the measured fractionations cannot be reconciled with the firstprinciple calculated equilibrium isotope fractionation factors regardless of the pairs of feldspars chosen [e.g., K/(K + Na) = 1/8, K/(K + Na) = 1/16, K/(K + Ca) = 1/8, or K/(K + Ca) = 1/32vs microcline]. Those pairs were chosen due to their closest match to the compositions in this study (see Table 1). These first-principle calculated equilibrium isotope fractionation factors were based on either local density approximation (LDA)^{30,31} or generalized gradient approximation (GGA)³⁸ methods, which are slightly different from each other (see Figure 4). Nevertheless, our measured fractionation does not match in either case, regardless the method used.

While the measured isotope fractionation between the phenocryst rim and matrix in the trachyandesite could certainly lend confidence to the calculated inter-mineral equilibrium isotope fractionation factors (see Figure 4B), which have not been independently verified with natural samples until this study, the disparity between the measured and calculated fractionations observed between the phenocryst core and matrix in the trachyandesite and between plagioclase and K-feldspar in

granite requires further discussion. This disparity can be explained by the following possibilities:

- (1) The measured fractionations do not represent equilibrium fractionations. This is not entirely surprising for the case of the phenocryst core and matrix in the trachyandesite. The large phenocryst cores (likely formed at depth) are not necessarily in chemical equilibrium with the surrounding melt (matrix) in the final storage location of a shallow magma chamber, just before eruption. The measured isotopic fractionation between the phenocryst core and matrix may thus be expected to be different from equilibrium fractionation. In contrast, the phenocryst rims are more likely to be in equilibrium with the melt as the rims crystallized in direct contact with the melt now interstitial to the phenocrystals. This may explain why the observed rim-matrix K isotope fractionation agrees with the ab initio calculation (see Figure 4B). Plagioclase feldspars are known for their complex kinetics of crystallization, so the large K isotope fractionation in the plagioclase of the granite may have led to larger than equilibrium isotope fractionations for K in the plagioclase. It has long been known that isotopes can be substantially fractionated by chemical diffusion, 42-53 a kinetic effect which has been observed in natural samples. 54,55 Depending on the direction in which K diffuses, the plagioclase can be enriched in heavier isotopes or lighter isotopes. Thus, the large fractionation observed in this granite sample could be due to the kinetic K isotopic fractionation.
- (2) The first-principle calculated equilibrium isotope fractionation factors were underestimated. Although the DFTbased equilibrium fractionation calculation has been shown to agree well with observations in natural samples for other isotopic systems, ⁵⁶ there has been no attempt to compare theoretical calculated K isotopic fractionation factors with observations in natural mineral samples. These theoretically calculated K isotopic fractionations have not been independently verified. The only approximation used in DFT calculations is the exchange correlation function. Two widely used approximations for the exchange correlation energy are the LDA^{30,31} or GGA,³⁸ which usually overestimate and underestimate the volume, respectively. GGA and LDA predict significantly different β -factors because the β -factors are sensitive to the bond length and hence to the volume. They produce similar inter-mineral equilibrium isotope fractionation factors.^{30,38} The volume variation of orthoclase is basically controlled by the variation of the K–O bond length because the SiO₄ or AlO₄ tetrahedron is hardly compressed. Thus, the disparity between the measured and calculated fractionations found in this study can be partly due to the pressure effect, which has not been evaluated yet in theoretical calculations. 30,31,38,39 Discrepancies between experimental and theoretical studies have also been found in other isotope systems. For example, ab initio calculations show that aragonite should be enriched in lighter Mg isotopes compared to calcite, ^{57–59} while experimental studies and natural samples show the opposite. ^{60–63} It has been shown that the symmetry of the lattice setting could have affected the ab initio calculations of aragonite.⁶⁴ Therefore, more

studies are needed to reconcile the difference between the measured and calculated fractionations in this study.

In summary, we have measured the apparent inter-mineral fractionations between plagioclase and potassium feldspars separated from one granite, one trachyandesite, and one gabbro. The observed inter-mineral fractionations are large in all three samples, implying that even at magmatic temperatures, the intermineral K isotopic fractionations can be confidently resolved with current high-precision K isotope analysis. While the measured isotope fractionation between the phenocryst rim and matrix in the trachyandesite matches well with the calculated inter-mineral equilibrium isotope fractionation factor, the measured fractionations between the phenocryst core and matrix in the trachyandesite and between the plagioclase and Kfeldspar are larger by a factor of $\sim 2-3$ than the ab initio calculated fractionation. This is most likely due to these minerals not reaching isotopic equilibrium, which is not uncommon in natural samples. Caution needs to be taken when applying the calculated equilibrium fractionation factors to natural samples as the system may (often) not be in chemical or isotopic equilibrium.

4.2. Implications for the K Isotopic Fractionation during Lunar Differentiation. The Lunar Magma Ocean (LMO) has been long known as a process that generated the anorthositic crust on Moon during the global-scale crystallization. 65,66 Our study and the ab initio calculations 30,31,38,39 predict large inter-mineral (and mineral-melt) K isotopic fractionations. It is possible that the LMO differentiation and the formation of the anorthositic crust on Moon would fractionate K isotopes as the Ca-rich and K-poor anorthositic plagioclases are expected to be significantly enriched in heavier K isotopes compared to other minerals and melts. The lunar crust might have been enriched in heavier K isotopes compared to its starting composition (presumably BSE) and the lunar mantle. Wang and Jacobsen³² found the K isotopic composition of Moon to be significantly heavier than that of Earth, and they interpreted the ~0.4% Earth-Moon difference as the consequence of Moon-forming giant impact. Nevertheless, this K isotopic difference between Earth and Moon could be alternatively explained by subsequent LMO differentiation. In this section, we discuss and model the K isotopic fractionation during LMO differentiation, particularly during the anorthite crystallization as other LMO cumulate minerals (e.g., olivine, orthopyroxene, clinopyroxene, spinel, ilmenite, and garnet) contain little K.⁶⁷ We then compare our modeled results to the measured K isotopic compositions of various lunar samples from the literature^{32,68} and evaluate whether the K isotopic fractionation during differentiation of LMO of the BSE composition alone can account for the observed difference in K isotopic compositions between Earth and Moon.

Lunar anorthite—melt K isotopic fractionation factor: the plagioclase accumulated from the LMO is primarily pure calcic plagioclase (anorthite). Potassium more readily substitutes in for Na than that for Ca, meaning the K content of lunar anorthite will be much lower than that of terrestrial plagioclases. Ion probe analyses of plagioclases from lunar anorthosites show K concentrations between 60 and 190 ppm. A large compilation of data for plagioclases from lunar ferroan anorthosites shows K_2O (wt %) between 0.01 and 0.03%. Thus, we can use the anorthite with a composition of K/(K + Ca) = 1/32 as the plagioclase in our case. We note that the composition of K/(K + Ca) = 1/32 is not the same as the lunar ferroan anorthite;

however, this is the lowest-K configuration (the closest to a lunar anorthite composition) that we could compute using this DFT method. ^{30,31} Zeng at al. ³⁸ also computed pure anorthite (no K) and anorthite with a composition of K/(K+Ca) = 1/8, and their results are slightly smaller than the computation in this study (see Figure 4A). This is due to the different approximation methods used by the two groups (LDA^{30,31} or GGA³⁸), with the LDA results being consistently larger than the GGA results (see Figure 4A). As shown in Figure 3, low-K and high-Ca plagioclases (e.g., K/(K + Ca) = 1/32) should have the shortest average K-O bond length and thus be most enriched in heavier K isotopes.^{30,31} Because the reduced partition function ratio $(10^3 \ln \beta)$ for silicate melts cannot be reliably computed, ³⁸ for our modeling, we selected the ab initio fractionation factor between anorthite (K/(K + Ca) = 1/32) and microcline as the Rayleigh fractionation factor (α). This is an approximation because it is not known whether the reduced partition function ratio for silicate melts would be the same as microcline or not. However, previously, Wang et al.³⁹ argued that because oxygen is the nearest to K in silicate melts, a K-feldspar unit may resemble the K-component in silicate melts. This is also due to the large K isotopic difference observed between Earth and Moon; thus, we wanted to use a maximum fractionation factor between common K minerals to evaluate the maximum effect due to the lunar differentiation (e.g., crystallization of plagioclase). Thus, we choose to use microcline as a proxy of the silicate melts.

First, we consider a general case of plagioclase-melt partitioning to determine how K concentrations in the residual melt change with the crystallization of plagioclase. To simplify the model, we assume that potassium behaves as a completely incompatible element through the initial stages of LMO crystallization when olivine and orthopyroxene cumulates form. These minerals do not incorporate K into their crystal lattices, with typical K concentrations being below the detection limit of an electron microprobe.⁶⁷ Although some K can be entrained in early cumulates in the interstices or melt inclusions, no isotopic fractionation between the trapped melts and LMO melt is expected. In addition, much higher crystallization temperatures of olivine and orthopyroxene than plagioclase $(1600 \,^{\circ}\text{C vs} \, 1200 \,^{\circ}\text{C})^{70}$ further reduce the isotopic fractionation between early cumulates and melts, if there were any. Therefore, we consider plagioclase as the only mineral that has significant effects on the K isotopic composition of the remaining melt. Previous studies^{71–75} have established a range of K partition coefficients D^{K} from 0.01 to 0.3 between plagioclase and melt. For this simple model, we assume the $D^{K} = 0.1$. The following equations describe the K concentration (ppm) as a function of the fraction (f) of the remaining melt during plagioclase crystallization

$$C_{\text{plag}} = 175.7 \times D \times (f)^{D-1} \tag{2}$$

$$C_{\text{melt}} = 175.7 \times (f)^{D-1}$$
 (3)

175.7 (ppm) is the starting K concentration in the melt after the crystallization of olivine and orthopyroxene, which is calculated from the K concentration of the bulk silicate Moon $(36.9 \pm 0.9 \text{ ppm})$, and the fraction of the early olivine and orthopyroxene cumulates from LMO (78% by volume) and mineral densities. $^{76-78}$ The mass fraction (f) of the remaining melt varies from 1 to 0.79 for plagioclase crystallization.

Second, we model the δ^{41} K in plagioclase and the residual melt as a function of plagioclase crystallization. For this simple model, we derived an α value (~1.0002) from the calculated fractionation factor (anorthite(K/(K + Ca) = 1/32) microcline)^{30,31} at temperatures ranging from 1200 to 1300 $^{\circ}$ C⁷⁰ (Figure 4). We also used an arbitrary α value (~1.0004) to evaluate how a larger fractionation factor would affect the K isotopic fractionation during LMO differentiation. Using these two α values, we apply the Rayleigh fractionation equations for the plagioclase and residual melt, respectively, as follows

$$\delta^{41} K_{plag} = 1000 \times [(f)^{\alpha - 1} \times \alpha - 1]$$
 (4)

$$\delta^{41}K_{\text{melt}} = 1000 \times ((f)^{\alpha - 1} - 1)$$
 (5)

The results of the modeled K concentrations and isotopic compositions of the plagioclases and remaining melt are shown in Figure 5a,b, respectively. We simplify the LMO crystallization

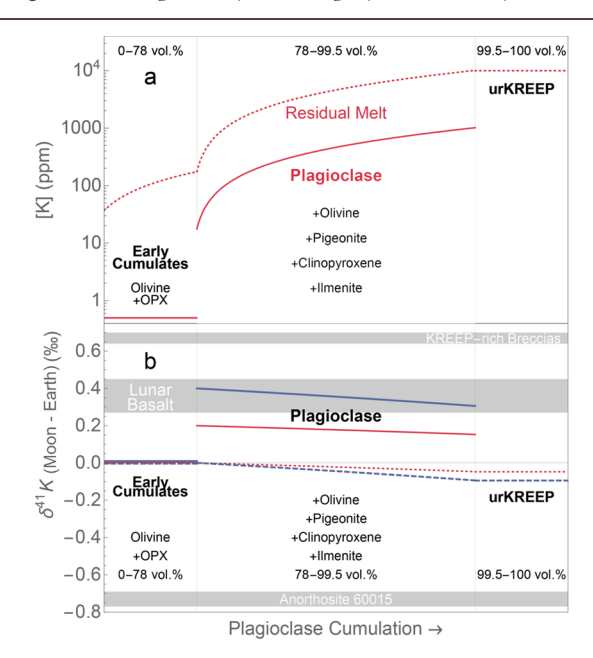


Figure 5. Fractional crystallization model of the evolution of (a) K concentrations and (b) K isotopic fractionation (Moon–Earth) during the LMO differentiation. The solid and dashed lines show evolution of cumulates and residual melts, respectively. The blue and red lines represent calculations based on two different plagioclase-melt isotopic fractionation factors (0.4 and 0.2%, respectively). This calculation is based on the magma ocean crystallization model by Snyder et al. The shaded areas represent measured K isotopic compositions of lunar basalts, KREEP-rich breccias, and anorthosite 60015.3

into three main stages based on Snyder et al.'s 77 original model: 0-78 vol % early cumulates (olivine and orthopyroxene), 78-99.5 vol % plagioclase, the other cumulates (olivine, pigeonite, clinopyroxene, and ilmenite), and the last 0.5 vol % final residual melt (i.e., urKREEP). 79 Given that K is highly incompatible, the K concentration in the residual melt increases by orders of magnitudes during LMO crystallization (Figure 5a), and the final residual melt is extremely rich in K (\sim 10,000 ppm vs the starting 36.9 ppm). 76 In contrast, despite the large K isotopic fractionation observed in plagioclase, the K isotopic compositions of the residual melt do not vary by more than 0.1% (Figure 5b) relative to the starting composition (i.e., BSE value). Because olivine and orthopyroxene only trap K in the interstices or as melt inclusions (no isotopic fractionation between trapped melts and LMO melt), we conclude the K isotopic composition of the lunar mantle (i.e., olivine and orthopyroxene cumulates)

Table 4. Measured K Isotope Ratios in NIST-SRM985 Compared to K Isotope Ratios in Planets, Igneous Rocks, and Minerals

	measured ⁴¹ K/ ³⁹ K	measured ⁴⁰ K/ ³⁹ K	measured $\delta^{41}\mathrm{K_{SRM985}}\left(\%_{o}\right)^{a}$	calculated $\delta^{^{40}} m K_{SRM985}~(\%)$	calculated ⁴⁰ K/ ³⁹ K	calculated ⁴⁰ K/K			
			NIST-SRM985						
Garner et al. ²⁴ + Naumenko et al. ⁸⁴ bulk planets	0.07216767	0.00012512	≡0	≡0	0.00012512	0.00011668			
bulk silicate Earth ³³			-0.807	-0.414	0.00012506	0.00011664			
bulk silicate Mars ^{29,92,93}			-0.667	-0.342	0.00012507	0.00011665			
bulk silicate Moon ^{32,68}			-0.447	-0.229	0.00012509	0.00011666			
bulk silicate Vesta ⁹²			-0.017	-0.009	0.00012511	0.00011668			
			Granite						
plagioclase			0.022	0.011	0.00012512	0.00011668			
K-feldspar			-0.841	-0.432	0.00012506	0.00011664			
biotite			-1.050	-0.539	0.00012505	0.00011663			
bulk			-0.808	-0.415	0.00012506	0.00011664			
			Trachyandesite						
phenocryst core			-0.648	-0.332	0.00012507	0.00011665			
phenocryst rim			-0.898	-0.461	0.00012506	0.00011663			
matrix			-0.928	-0.476	0.00012506	0.00011663			
bulk			-0.862	-0.442	0.00012506	0.00011664			
Gabbro									
plagioclase			-0.396	-0.203	0.00012509	0.00011666			
bulk			-0.727	-0.373	0.00012507	0.00011664			

^aThe data were converted to use SRM985 as a reference for δ^{41} K-values, rather than Suprapur or SRM3141a using the value for this standard in Table 3.

should not have been fractionated during the LMO differentiation (Figure 5b).

We also compared the model K isotopic compositions of lunar basalts, KREEP-rich breccias, and the anorthositic crust with the measured values of lunar samples (see Figure 5b).⁶⁸ As the early cumulates, olivine and orthopyroxene show no fractionation from the starting BSE composition. Lunar basalts, partial melts of lunar mantle, should also have no measurable (<0.1%o) K isotopic fractionation compared to the BSE value, which does not agree with measurements of lunar basalts (see Figure 5b).⁶⁸ The final residual melt of LMO formed the urKREEP. 79 Our model predicts slightly lighter compositions (see Figure 5b). Again, these model values for urKREEP are inconsistent with the measurements, where KREEP-rich breccias show a significantly elevated value (see Figure 5b).⁶⁸ Only one lunar anorthosite sample (60015) has been analyzed for K isotopes by Humayun and Clayton⁸⁰ and Tian et al.,⁶⁸ which is much lighter than the modeled values (see Figure 5b). Tian et al.⁶⁸ interpreted this light K isotope enrichment in anorthosites as a result of recondensation of isotopically light vapor back to the surface of Moon and incorporation into the K-poor anorthosites (thus dominating the K isotopic signatures).

In summary, we modeled the K isotopic fractionation during LMO differentiation, particularly focused on the formation of the anorthositic crust, as we have observed large K isotopic fractionation among terrestrial plagioclases. However, the modeled results do not match the measured values in lunar samples, which shows that the LMO differentiation cannot generate the observed K isotopic difference between Earth and Moon, as well as the fractionations among different lunar samples. Other processes such as evaporation and recondensation during Moon-forming giant impact and magmatic degassing are required. ^{32,68,80,81}

4.3. Implication on the K–Ca–Ar Dating System. We found large inter-mineral K isotopic fractionations in all three igneous rocks examined (Figure 1). Potassium has three

isotopes, with only ⁴⁰K being radioactive. Potassium-40 has two decay products: β^+ decay to ⁴⁰Ar with a half-life of 1.248 billion years ($\lambda_\varepsilon = 5.81 \times 10^{-11} \, \mathrm{yr}^{-1}$) and β^- decay to ⁴⁰Ca ($\lambda_\beta = 4.96 \times 10^{-10} \, \mathrm{yr}^{-1}$). ⁸² Incorporating these constants into the well-established decay equation, ⁸³ the number of ⁴⁰Ar nuclides N at any given time will be

$$N_{40_{\text{Ar}}}(t) = N_{40_{\text{Ar}}}(0) + \frac{\lambda_{\varepsilon}}{\lambda_{\varepsilon} + \lambda_{\beta}} N_{40_{\text{K}}}(t) [e^{(\lambda_{\varepsilon} + \lambda_{\beta})t} - 1]$$
(6)

The term $\frac{\lambda_{\varepsilon}}{\lambda_{\varepsilon} + \lambda_{\beta}}$ reflects the proportion of 40 K atoms taking the

 40 Ar pathway and is equal to the branching ratio of 10.5%. 82 The number of ⁴⁰K parent nuclides is obtained from the K elemental concentration, assuming that the ⁴⁰K isotopic abundance in all samples is fixed. The 40 K isotopic abundance (40 K/K = 116.7 \pm 0.4 ppm), as measured in the NIST standard SRM985 by Garner et al.,²⁴ was assumed to apply to all terrestrial samples; it was recently revised to 116.68 ± 0.08 ppm by Naumenko et al.⁸⁴ Since we have observed significant K isotopic fractionations among minerals in the rock samples reported here, this assumption needs to be re-evaluated. In this section, we calculate new 40K isotopic abundances (40K/K ratios) for different minerals and rocks and discuss their potential influence on the K-Ar dating. We note that although only K-Ar dating is explicitly discussed here, the ⁴⁰Ar-³⁹Ar dating ("K-Ar dating by activation with fast neutrons") 85 is similarly affected by K isotopic fractionations among minerals.

Here, we report the δ^{41} K values relative to the NIST-SRM3141a (see Table 3). Thus, we need to recalculate our δ^{41} K values relative to NIST-SRM985, the international K isotopic standard.² There is no direct comparison between NIST-SRM3141a and NIST-SRM985. NIST-SRM985 is discontinued and cannot be easily acquired. However, we can link the NIST-SRM3141a with the NIST-SRM985 through seawater. Morgan et al.⁴ reported a 0.259 \pm 0.069% difference between the NIST-SRM985 and seawater. Wang et al.³⁴ reported a 0.118 \pm

0.071% difference between the seawater and NIST-SRM3141a. Thus, we can recalculate our measured δ^{41} K values relative to the NIST-SRM985 as δ^{41} K_{SRM985} = δ^{41} K_{SRM3141a} - 0.377 (±0.099; Table 4).

In order to calculate 40 K isotopic abundances (40 K/K ratios), we also need to calculate δ^{40} K $_{SRM985}$ from δ^{41} K $_{SRM985}$ based on the mass-dependent fractionation law, 86,87 as follows

$$\alpha_{40/39} = (\alpha_{41/39})^{\beta} \tag{7}$$

for equilibrium fractionation:
$$\beta = \frac{\left(\frac{1}{i} - \frac{1}{j}\right)}{\left(\frac{1}{k} - \frac{1}{j}\right)} = 0.5131$$
(8)

for kinetic fractionation:
$$\beta = \frac{\ln \frac{i}{j}}{\ln \frac{k}{j}} = 0.5069$$
 (9)

where i, j, and k are the respective K isotopic masses of 40, 39, and 41. For small ranges of fractionation (such as the maximum of ~1‰ in this study), the fractionation equation can be approximated by $\delta^{40}K = \beta \cdot \delta^{41}K$, with β as the slope in K three-isotope plot ($\delta^{40}K_{SRM985}$ vs $\delta^{41}K_{SRM985}$; Figure 6). We have used the equilibrium fractionation, but both equilibrium and kinetic fractionation yield very similar results.

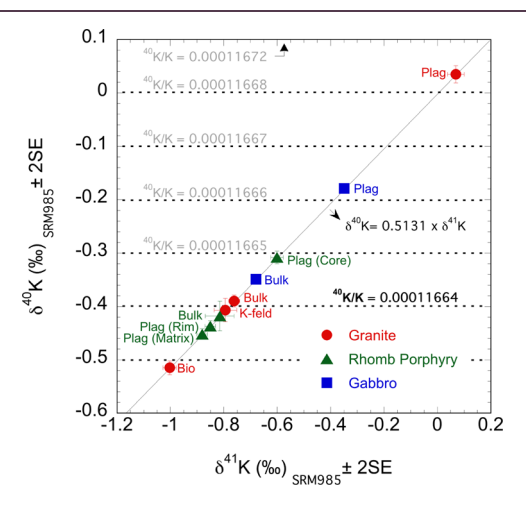


Figure 6. Potassium three-isotope plot for igneous rocks and minerals in this study. The $\delta^{41}K_{SRM985}$ values are converted from the measured $\delta^{41}K_{Suprapur}$ values. 4,29,34 $\delta^{40}K_{SRM985}$ values are calculated by assuming mass-dependent fractionation law $(\delta^{40}K_{SRM985}=0.5131\times\delta^{41}K_{SRM985}).$ The corresponding $^{40}K/K$ values are also plotted as dashed lines. The $^{40}K/K$ value (0.00011672) for NIST-SRM985 ($\delta^{40}K_{SRM985}=0$) is obtained from a study by Garner et al. 24 A refined $^{40}K/K$ value (0.00011664) is proposed here as a better representative value for igneous rocks and minerals (except for some plagioclases).

Table 4 reports the calculated $\delta^{40}K_{SRM985}$ for each sample in this study and their corresponding $^{40}K/K$ ratios. The newly calculated $^{40}K/K$ ratios for igneous minerals and rocks vary from 0.00011663 to 0.00011668, clearly deviating from the conventional value of 0.0001167(2). This deviation is primarily due to the fact that the international K isotopic standard NIST-SRM985 is not a good representative of the BSE. Although NIST-SRM985's value is closer to the K isotopic compositions of seawater and sylvites, characteristic of the isotopic signature of samples experienced low-temperature alteration compared to

the BSE. 14,17,34,88 Therefore, we propose a refined 40 K/K ratio of 0.00011664 \pm 0.00000011 (116.64 \pm 0.11 ppm) as the representative 40 K isotopic composition of the BSE (see Figure 6 and Table 4). However, we want to note that this value is only the "average" isotopic composition of the BSE. For each mineral or rock, the actual 40 K/K ratio could be different from this "average" value (see Figure 6). In principle, one may have to determine the 39 K/ 40 K (41 K/ 39 K) in every sample to be dated with either K–Ar or Ar/Ar techniques, and the actual 40 K/K ratios should be used in the age calculation.

As mentioned before, one of the assumptions for K–Ar dating is that the 40 K/K ratio must be constant at any given time, fixed at 0.0001167(2) at present day. ⁸⁹ However, we showed that the 40 K/K ratios are not fixed, so this assumption is no longer valid. The calculated 40 K/K ratios vary from 0.00011663 in biotite to 0.00011668 in plagioclase even within the same granite rock sample (see Figure 6). We will now consider how much this change in the 40 K/K ratio affects the K–Ar ages. We can derive a relationship between time τ using either the conventional 40 K/K ratio of 0.00011672 24 or the new 40 K/K ratios (0.00011663 to 0.00011668) to evaluate the errors caused by possible K isotopic fractionation. Time τ can be derived from the previously defined K–Ar decay equation

$$\tau = \frac{1}{\lambda} \ln \left[1 + \frac{\lambda}{\lambda_{\varepsilon}} \frac{^{40} \text{Ar}^*}{^{40} \text{K}} \right]$$
 (10)

where $\lambda = \lambda_{\varepsilon} + \lambda_{\beta}$.

Equation 10 can be taken to represent a sample dated using the conventional 40 K/K ratio and can be modified with a "correction factor", which we designate as c. It can be defined as the revised 40 K/K ratio divided by the conventional 40 K/K ratio, as assumed previously.

$$c = \frac{^{40}\text{K/K}_{\text{new}}}{^{40}\text{K/K}_{\text{old}}} \tag{11}$$

Then, the new equation is

$$\tau_{\text{new}} = \frac{1}{\lambda} \ln \left[1 + \frac{\lambda}{\lambda_{\varepsilon}} \frac{^{40}\text{Ar}^*}{^{40}\text{K}} \frac{1}{c} \right]$$
(12)

with the ⁴⁰K here still referring to the conventional ⁴⁰K abundance commonly assumed and multiplied by the "correction" factor c. Using eq 10 again, the common factor across the two time equations, namely $\frac{\lambda}{\lambda_{\varepsilon}} \frac{^{40} \text{Ar}^*}{^{40} \text{K}}$, can be written in terms of τ_{old} and substituted.

$$e^{\lambda \tau_{\text{old}}} - 1 = \frac{\lambda}{\lambda_{\varepsilon}} \frac{^{40}\text{Ar*}}{^{40}\text{K}}$$
 (13)

$$\tau_{\text{new}} = \frac{1}{\lambda} \ln \left[1 + \left(e^{\lambda \tau_{\text{old}}} - 1 \right) \frac{1}{c} \right] \tag{14}$$

The percent error will clearly not remain constant over time because the τ functions are not linear. A graph (Figure 7) of the percent difference between the two ages plotted as a function of τ_1 from 0 to 4.567 billion years (Ga) shows that the percent error decreases as τ_1 increases. The age error is calculated as $\left(\frac{\tau_{\rm new}}{\tau_{\rm old}}-1\right)\times 100$. This gives us the following equation

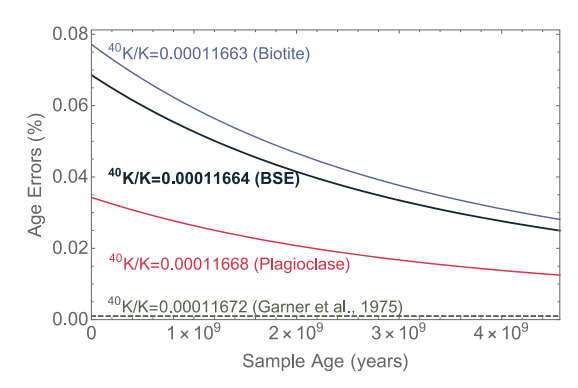


Figure 7. Percent error on samples dated using the conventional 40 K/K ratio $(0.00011672)^{24}$ vs using new 40 K/K ratios (0.00011663, 0.00011664 to 0.00011668). The maximum errors vary from $\sim 0.08\%$ in the youngest rocks to $\sim 0.03\%$ in rocks as old as the solar system. This means a rock dated on an order of magnitude 10^6 (million years) will require around an 800-year correction, while a rock dated on the order of 10^9 (billion years) will require a 500,000- to 1,200,000-year correction (see Figure 8).

$$y = \left(\frac{\tau_{\text{new}}}{\tau_{\text{old}}} - 1\right) \times 100$$
$$= \left[\frac{1}{\lambda \tau_{\text{old}}} \ln \left[1 + \left(e^{\lambda \tau_{\text{old}}} - 1\right) \frac{1}{c}\right] - 1\right] \times 100$$
(15)

The percent error over time decreases in an exponential-like way from an initial maximum error of around 0.08% today to a maximum error of 0.03% at the age of the solar system.

To demonstrate how that affects absolute ages, Figure 8 shows the age difference $(\tau_{\rm new} - \tau_{\rm old})$ for samples dated using the

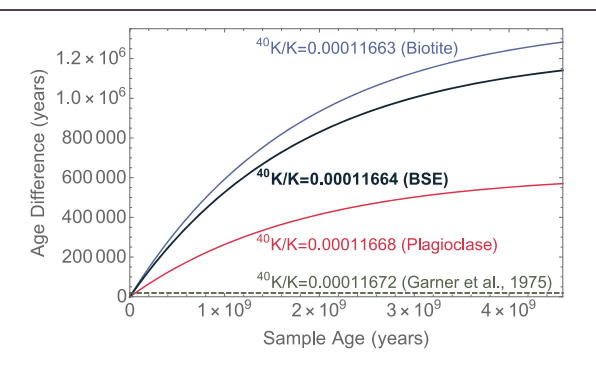


Figure 8. Age difference $(\tau_2 - \tau_1)$ on samples dated using the conventional $^{40}{\rm K/K}$ ratio $(0.00011672)^{24}$ vs using new $^{40}{\rm K/K}$ ratios $(0.00011663,\,0.00011664$ to 0.00011668). Even though the percent error over time decreases with increased rock age, the error itself increases.

conventional 40 K/K ratio (0.00011672) and new 40 K/K ratios (0.00011663, 0.00011664 to 0.00011668). For a rock of a few Ma old, the new age ($\tau_{\rm new}$) is \sim 800-year older than the previous one ($\tau_{\rm old}$), while for a rock of a few billion years old, the new age ($\tau_{\rm new}$) is \sim 500,000 to 1,200,000-year older than the previous one ($\tau_{\rm old}$). The 1,200,000 year error at the beginning of the solar system is much larger than the uncertainty in 207 Pb/ 206 Pb ages for this early time.

To provide a simple way to estimate the influence of different 40 K/K ratios on the ages, here we also provide an approximation for eq 15, as derived below.

Equation 10 can be rewritten as

$$\tau = \frac{1}{\lambda} \ln \left[1 + \frac{\lambda}{\lambda_{\varepsilon}} \frac{^{40}\text{Ar*}/\text{K}}{^{40}\text{K}/\text{K}} \right]$$
 (16)

The derivative of τ is

$$\tau'\left(\frac{^{40}K}{K}\right) = -\frac{\frac{^{40}Ar^*}{\lambda_{\varepsilon} \cdot K}}{\frac{^{40}K}{K} \cdot \left(\frac{\lambda^{\cdot 40}Ar^*}{\lambda_{\varepsilon} \cdot K} + \frac{^{40}K}{K}\right)}$$
(17)

which can be simplified into

$$\tau'\left(\frac{^{40}K}{K}\right) = -\frac{1}{\lambda \frac{^{40}K}{K} + \lambda_{\varepsilon} \frac{^{40}K}{K} \cdot \frac{^{40}K}{^{40}Ar^*}}$$
(18)

The change of ⁴⁰K/K ratios is

$$\Delta \left(\frac{^{40}\text{K}}{\text{K}}\right) = \left(\frac{^{40}\text{K}}{\text{K}}\right)_{\text{new}} - \left(\frac{^{40}\text{K}}{\text{K}}\right)_{\text{old}} \tag{19}$$

Because the new $^{40} K/K$ ratios (0.00011663, 0.00011664 to 0.00011668) are very close to the conventional $^{40} K/K$ ratio (0.00011672), the $\Delta \left(\frac{^{40} K}{K}\right)$ is small; thus, we could approximate the change of $\tau(\tau_{\rm new}-\tau_{\rm old})$

$$\Delta \tau = \tau' \left(\frac{^{40}K}{K} \right) \cdot \Delta \left(\frac{^{40}K}{K} \right) \tag{20}$$

Substituting eq 18 into eq 20

$$\Delta \tau = -\frac{1}{\lambda \frac{{}^{40}K}{K} + \lambda_{\varepsilon} \frac{{}^{40}K}{K} \cdot \frac{{}^{40}K}{{}^{40}Ar} \cdot \Delta \left(\frac{{}^{40}K}{K}\right)}$$
(21)

and rearranging eq 10

$$\frac{^{40}\text{K}}{^{40}\text{Ar}^*} = \frac{\lambda}{\lambda_{\scriptscriptstyle F}(e^{\lambda\tau} - 1)} \tag{22}$$

Equation 21 can be rewritten as

$$\Delta \tau = \frac{(1 - e^{\lambda \tau})}{\lambda \frac{{}^{40}K}{K} e^{\lambda \tau}} \cdot \Delta \left(\frac{{}^{40}K}{K}\right)$$
(23)

The percentage age error can be written as

$$y = 100 \times \frac{\Delta \tau}{\tau} = \frac{(1 - e^{\lambda \tau})}{\lambda \tau \frac{{}^{40}K}{K}} e^{\lambda \tau} \cdot \Delta \left(\frac{{}^{40}K}{K}\right) \times 100$$
 (24)

We have compared the approximation equations with the more exact equations (see Supporting Information, Figure S1) and shown that they yield identical results (i.e., percentage age error).

In summary, the uncertainty of 40 K/K is only one of many factors that contribute to the overall K–Ar age uncertainty. The revision of 40 K/K ratio would generate a maximum 0.08% error for young rocks and 0.03% for old rocks (Figure 7) that are not significant compared to the typical level of analytical uncertainty (\sim 0.1%) of K–Ar dating. Although currently the uncertainty caused by different 40 K/K ratios may be safely negligible, future improvements of K–Ca–Ar methods may require this 40 K/K variability to be taken into account.

5. CONCLUSIONS

We report large (up to $\sim 1\%$) inter-mineral K isotope fractionations between common K-bearing minerals separated from three representative igneous rocks (one granite, one trachyandesite, and one gabbro). In particular, plagioclases are universally enriched in heavier K isotopes compared to potassium feldspars and other minerals, consistent with the direction of isotopic fractionation predicted by ab initio calculations. While the measured isotope fractionation between the phenocryst rim and matrix in the trachyandesite matches quantitively with the calculated inter-mineral equilibrium isotope fractionation factor, the measured K isotope fractionations between the phenocryst core and the matrix in the trachyandesite and between plagioclase and K-feldspar in granite are significantly larger than the theoretically calculated fractionation factors. We attribute this discrepancy to nonequilibrium conditions in nature. Nevertheless, the accuracy and validity of the theoretical calculations based on DFT still have to be tested by more natural samples or experimental data in addition to this study.

We modeled the K isotopic fractionation during the LMO differentiation and found only a negligible effect on the K isotopic composition of the lunar mantle. Thus, K isotopic fractionation during formation of the lunar anorthositic crust is unlikely to cause the large K isotopic difference between Earth and Moon, as well as among different lunar samples. Alternative processes, such as evaporation and recondensation during Moon-forming giant impact and magmatic degassing, are required.

Moreover, our results help improve the accuracy of the K–Ca–Ar dating technique. The K isotopic variations observed here show that the assumption of a constant $^{41}{\rm K}/^{39}{\rm K}$ ratio in all rocks and minerals is no longer valid. We propose a new $^{40}{\rm K}/{\rm K}$ ratio of 0.00011664 \pm 0.00000011 (116.64 \pm 0.11 ppm), which represents the BSE, instead of the conventional value of 0.0001167(2), which is similar to seawater. We also show that further improvement of accuracy of the K–Ca–Ar chronology systems requires measurements of the samples' K isotope compositions. However, at current analytical uncertainty of K–Ar dating, the K isotopic fractionation between minerals is still a second-order effect on the precision of K–Ar dating.

ASSOCIATED CONTENT

Supporting Information

The Supporting Information is available free of charge at https://pubs.acs.org/doi/10.1021/acsearthspace-chem.1c00147.

Figures showing percent error using conventional versus new $^{40}\text{K/K}$ ratios, and the age difference $(\tau_2-\tau_1)$ using conventional versus new $^{40}\text{K/K}$ ratios (PDF)

Electron microprobe analysis data for minerals in granite and trachyandesite (XLSX)

AUTHOR INFORMATION

Corresponding Author

Kun Wang — Department of Earth and Planetary Sciences, Harvard University, Cambridge, Massachusetts 02138, United States; Department of Earth and Planetary Sciences, McDonnell Center for the Space Sciences, Washington University in St. Louis, St. Louis, Missouri 63130, United States; ⊚ orcid.org/0000-0003-0691-7058;

Email: wangkun@wustl.edu

Authors

- W. Wilson Kuhnel Department of Earth and Planetary Sciences, Harvard University, Cambridge, Massachusetts 02138, United States
- Stein B. Jacobsen Department of Earth and Planetary Sciences, Harvard University, Cambridge, Massachusetts 02138, United States
- Yonghui Li Laboratory of Seismology and Physics of Earth's Interior, School of Earth and Space Sciences, University of Science and Technology of China, Hefei, Anhui 230026, China
- Yaray Ku Department of Earth and Planetary Sciences, Harvard University, Cambridge, Massachusetts 02138, United States
- Michail I. Petaev Department of Earth and Planetary Sciences, Harvard University, Cambridge, Massachusetts 02138, United States
- Shichun Huang Department of Geoscience, University of Nevada, Las Vegas, Nevada 89154, United States
- Zhongqing Wu Laboratory of Seismology and Physics of Earth's Interior, School of Earth and Space Sciences, University of Science and Technology of China, Hefei, Anhui 230026, China; CAS Center for Excellence in Comparative Planetology, University of Science and Technology of China, Hefei, Anhui 230026, China

Complete contact information is available at: https://pubs.acs.org/10.1021/acsearthspacechem.1c00147

Notes

The authors declare no competing financial interest.

ACKNOWLEDGMENTS

K.W. thanks the McDonnell Center for the Space Sciences, the Harvard Origins of Life initiative, and NASA (Emerging Worlds Program grant number #80NSSC21K0379) for their financial support. Z.W. is supported by the Strategic Priority Research Program (B) of the Chinese Academy of Sciences (XDB41000000). S.H. acknowledges support from NSF (EAR-1942042). S.B.J. acknowledges support from NASA (Emerging Worlds Program grant number #80NSSC20K0346). We appreciate valuable discussions with Drs. Brad Jolliff, Paul Carpenter, Mike Krawczynski, and Rita Parai. Reviews by anonymous referee helped shape the discussion in this study. Editorial handling and additional comments by Prof. Sumit Chakraborty are also acknowledged.

■ REFERENCES

- (1) Rudnick, R. L.; Gao, S. Composition of the Continental Crust. In *Treatise on Geochemistry*, 2nd ed; Holland, H. D., Turekian, K. K., Eds.; Elsevier: Oxford, 2014; pp 1–51.
- (2) Meija, J.; Coplen, T. B.; Berglund, M.; Brand, W. A.; De Bièvre, P.; Gröning, M.; Holden, N. E.; Irrgeher, J.; Loss, R. D.; Walczyk, T.; Prohaska, T. Atomic Weights of the Elements 2013 (IUPAC Technical Report). *Pure Appl. Chem.* **2016**, *88*, 265.
- (3) Humayun, M.; Clayton, R. N. Precise Determination of the Isotopic Composition of Potassium: Application to Terrestrial Rocks and Lunar Soils. *Geochim. Cosmochim. Acta* 1995, 59, 2115–2130.
- (4) Morgan, L. E.; Santiago Ramos, D. P.; Davidheiser-Kroll, B.; Faithfull, J.; Lloyd, N. S.; Ellam, R. M.; Higgins, J. A. High-Precision 41 K/ 39 K Measurements by MC-ICP-MS Indicate Terrestrial Variability of δ^{41} K. *J. Anal. At. Spectrom.* **2018**, 33, 175–186.
- (5) Chen, H.; Tian, Z.; Tuller-Ross, B.; Korotev, R. L.; Wang, K. High-Precision Potassium Isotopic Analysis by MC-ICP-MS: An Inter-Laboratory Comparison and Refined K Atomic Weight. *J. Anal. At. Spectrom.* **2019**, *34*, 160–171.

- (6) Wang, K.; Peucker-Ehrenbrink, B.; Chen, H.; Lee, H.; Hasenmueller, E. A. Dissolved Potassium Isotopic Composition of Major World Rivers. *Geochim. Cosmochim. Acta* **2021**, 294, 145–159.
- (7) Wang, K.; Jacobsen, S. B. An Estimate of the Bulk Silicate Earth Potassium Isotopic Composition Based on MC-ICPMS Measurements of Basalts. *Geochim. Cosmochim. Acta* **2016**, *178*, 223–232.
- (8) Li, W.; Beard, B. L.; Li, S. Precise Measurement of Stable Potassium Isotope Ratios Using a Single Focusing Collision Cell Multi-Collector ICP-MS. J. Anal. At. Spectrom. 2016, 31, 1023–1029.
- (9) Moynier, F.; Hu, Y.; Wang, K.; Zhao, Y.; Gérard, Y.; Deng, Z.; Moureau, J.; Li, W.; Simon, J. I.; Teng, F.-Z. Potassium Isotopic Composition of Various Samples Using a Dual-Path Collision Cell-Capable Multiple-Collector Inductively Coupled Plasma Mass Spectrometer, Nu Instruments Sapphire. *Chem. Geol.* **2021**, *571*, 120144.
- (10) Hu, Y.; Chen, X.-Y.; Xu, Y.-K.; Teng, F.-Z. High-Precision Analysis of Potassium Isotopes by HR-MC-ICPMS. *Chem. Geol.* **2018**, 493, 100–108.
- (11) Li, W.; Li, S.; Beard, B. L. Geological Cycling of Potassium and the K Isotopic Response: Insights from Loess and Shales. *Acta Geochim.* **2019**, *38*, 508–516.
- (12) Huang, T.-Y.; Teng, F.-Z.; Rudnick, R. L.; Chen, X.-Y.; Hu, Y.; Liu, Y.-S.; Wu, F.-Y. Heterogeneous Potassium Isotopic Composition of the Upper Continental Crust. *Geochim. Cosmochim. Acta* **2019**, 278, 122–136.
- (13) Wang, K.; Li, W.; Li, S.; Tian, Z.; Koefoed, P.; Zheng, X.-Y. Geochemistry and Cosmochemistry of Potassium Stable Isotopes. *Geochemistry* **2021**, *81*, 125786.
- (14) Chen, H.; Liu, X.-M.; Wang, K. Potassium Isotope Fractionation during Chemical Weathering of Basalts. *Earth Planet. Sci. Lett.* **2020**, 539, 116192.
- (15) Parendo, C. A.; Jacobsen, S. B.; Wang, K. K Isotopes as a Tracer of Seafloor Hydrothermal Alteration. *Proc. Natl. Acad. Sci.* **2017**, *144*, 1827.
- (16) Santiago Ramos, D. P.; Morgan, L. E.; Lloyd, N. S.; Higgins, J. A. Reverse Weathering in Marine Sediments and the Geochemical Cycle of Potassium in Seawater: Insights from the K Isotopic Composition (⁴¹K/³⁹K) of Deep-Sea Pore-Fluids. *Geochim. Cosmochim. Acta* **2018**, 236, 99–120.
- (17) Li, S.; Li, W.; Beard, B. L.; Raymo, M. E.; Wang, X.; Chen, Y.; Chen, J. K isotopes as a tracer for continental weathering and geological K cycling. *Proc. Natl. Acad. Sci. U.S.A.* **2019**, *116*, 8740–8745.
- (18) Teng, F.-Z.; Hu, Y.; Ma, J.-L.; Wei, G.-J.; Rudnick, R. L. Potassium Isotope Fractionation during Continental Weathering and Implications for Global K Isotopic Balance. *Geochim. Cosmochim. Acta* **2020**, 278, 261–271.
- (19) Liu, H.; Xue, Y.-Y.; Zhang, G.; Sun, W.-D.; Tian, Z.; Tuller-Ross, B.; Wang, K. Potassium Isotopic Composition of Low-Temperature Altered Oceanic Crust and Its Impact on the Global K Cycle. *Geochim. Cosmochim. Acta* **2021**, 311, 59–73.
- (20) Li, W.; Liu, X.-M.; Wang, K.; Joel Fodrie, F.; Yoshimura, T.; Hu, Y.-F. Potassium Phases and Isotopic Composition in Modern Marine Biogenic Carbonates. *Geochim. Cosmochim. Acta* **2021**, *304*, 364.
- (21) Li, W.; Liu, X.-M.; Hu, Y.; Teng, F.-Z.; Hu, Y. Potassium Isotopic Fractionation during Clay Adsorption. *Geochim. Cosmochim. Acta* **2021**, 304, 160–177.
- (22) Li, W.; Liu, X.-M.; Wang, K.; Koefoed, P. Lithium and Potassium Isotope Fractionation during Silicate Rock Dissolution: An Experimental Approach. *Chem. Geol.* **2021**, *568*, 120142.
- (23) Morgan, L. E.; Tappa, M.; Ellam, R.; Mark, D.; Higgins, J.; Simon, J. Potassium Isotopic Compositions of NIST Potassium Standards and ⁴⁰Ar/³⁹Ar Mineral Standards. In *American Geophysical Union Fall Meeting*, 2013.
- (24) Garner, E. L.; Murphy, T. J.; Gramlich, J. W.; Paulsen, P. J.; Barnes, I. L. Absolute Isotopic Abundance Ratios and the Atomic Weight of a Reference Sample of Potassium. *J. Res. Natl. Bur. Stand., Sect. A* 1975, 79, 713–725.
- (25) Trønnes, R. G.; Brandon, A. D. Mildly Peraluminous High-Silica Granites in a Continental Rift: The Drammen and Finnemarka

- Batholiths, Oslo Rift, Norway. *Contrib. Mineral. Petrol.* **1992**, 109, 275–294.
- (26) Jacobsen, S. B.; Wasserburg, G. J. Nd and Sr Isotopic Study of the Permian Oslo Rift. *U.S. Geological Survey Open File Report*, 1978; Vol. 78–701, pp 194–196.
- (27) Neumann, E.-R.; Larsen, B. T.; Sundvoll, B. Compositional Variations among Gabbroic Intrusions in the Oslo Rift. *Lithos* **1985**, *18*, 35–59.
- (28) Strelow, E. W. E.; Toerien, F. .; Weinert, C. H. S. W. Accurate Determination of Traces of Sodium and Potassium in Rocks by Ion Exchange Followed by Atomic Absorption Spectroscopy. *Anal. Chim. Acta* **1970**, *50*, 399–405.
- (29) Ku, Y.; Jacobsen, S. B. Potassium Isotope Anomalies in Meteorites Inherited from the Protosolar Molecular Cloud. *Sci. Adv.* **2020**, *6*, No. eabd0511.
- (30) Li, Y.; Wang, W.; Huang, S.; Wang, K.; Wu, Z. First-Principles Investigation of the Concentration Effect on Equilibrium Fractionation of K Isotopes in Feldspars. *Geochim. Cosmochim. Acta* **2019**, 245, 374—384.
- (31) Li, Y.; Wang, W.; Wu, Z.; Huang, S. First-Principles Investigation of Equilibrium K Isotope Fractionation among K-Bearing Minerals. *Geochim. Cosmochim. Acta* **2019**, *264*, 30–42.
- (32) Wang, K.; Jacobsen, S. B. Potassium Isotopic Evidence for a High-Energy Giant Impact Origin of the Moon. *Nature* **2016**, 538, 487–490.
- (33) Tuller-Ross, B.; Marty, B.; Chen, H.; Kelley, K. A.; Lee, H.; Wang, K. Potassium Isotope Systematics of Oceanic Basalts. *Geochim. Cosmochim. Acta* **2019**, 259, 144–154.
- (34) Wang, K.; Close, H. G.; Tuller-Ross, B.; Chen, H. Global Average Potassium Isotope Composition of Modern Seawater. *ACS Earth Space Chem.* **2020**, *4*, 1010–1017.
- (35) Hille, M.; Hu, Y.; Huang, T.-Y.; Teng, F.-Z. Homogeneous and Heavy Potassium Isotopic Composition of Global Oceans. *Sci. Bull.* **2019**, *64*, 1740–1742.
- (36) Tuller-Ross, B.; Savage, P. S.; Chen, H.; Wang, K. Potassium Isotope Fractionation during Magmatic Differentiation of Basalt to Rhyolite. *Chem. Geol.* **2019**, *525*, 37–45.
- (37) Schauble, E. A. Applying Stable Isotope Fractionation Theory to New Systems. In *Geochemistry of Non-Traditional Stable Isotopes, Reviews in Mineralogy & Geochemistry*; Johnson, C. M., Beard, B. L., Albarede, F., Eds.; Mineralogical Soc America: Washington, 2004; Vol. 55, pp 65–112.
- (38) Zeng, H.; Rozsa, V. F.; Nie, N. X.; Zhang, Z.; Pham, T. A.; Galli, G.; Dauphas, N. Ab Initio Calculation of Equilibrium Isotopic Fractionations of Potassium and Rubidium in Minerals and Water. ACS Earth Space Chem. 2019, 3, 2601–2612.
- (39) Wang, X.; Fitoussi, C.; Bourdon, B.; Fegley, B.; Charnoz, S. Tin Isotopes Indicative of Liquid—Vapour Equilibration and Separation in the Moon-Forming Disk. *Nat. Geosci.* **2019**, *12*, 707—711.
- (40) Bigeleisen, J.; Mayer, M. G. Calculation of Equilibrium Constants for Isotopic Exchange Reactions. *J. Chem. Phys.* **1947**, *15*, 261–267.
- (41) Urey, H. C. The Thermodynamic Properties of Isotopic Substances. *J. Chem. Soc.* **1947**, 562–581.
- (42) Schoen, A. H. Correlation and the Isotope Effect for Diffusion in Crystalline Solids. *Phys. Rev. Lett.* **1958**, *1*, 138–140.
- (43) Tsuchiyama, A.; Kawamura, K.; Nakao, T.; Uyeda, C. Isotopic Effects on Diffusion in MgO Melt Simulated by the Molecular Dynamics (MD) Method and Implications for Isotopic Mass Fractionation in Magmatic Systems. *Geochim. Cosmochim. Acta* 1994, 58, 3013–3021.
- (44) Collinet, M.; Charlier, B.; Namur, O.; Oeser, M.; Médard, E.; Weyer, S. Crystallization History of Enriched Shergottites from Fe and Mg Isotope Fractionation in Olivine Megacrysts. *Geochim. Cosmochim. Acta* 2017, 207, 277–297.
- (45) Teng, F.-Z.; McDonough, W. F.; Rudnick, R. L.; Walker, R. J. Diffusion-Driven Extreme Lithium Isotopic Fractionation in Country Rocks of the Tin Mountain Pegmatite. *Earth Planet. Sci. Lett.* **2006**, 243, 701–710.

- (46) Richter, F. M.; Davis, A. M.; DePaolo, D. J.; Watson, E. B. Isotope Fractionation by Chemical Diffusion between Molten Basalt and Rhyolite. *Geochim. Cosmochim. Acta* **2003**, *67*, 3905–3923.
- (47) Richter, F. M.; Liang, Y.; Davis, A. M. Isotope Fractionation by Diffusion in Molten Oxides. *Geochim. Cosmochim. Acta* **1999**, *63*, 2853–2861.
- (48) Roskosz, M.; Luais, B.; Watson, H. C.; Toplis, M. J.; Alexander, C. M. O. 'D.; Mysen, B. O. Experimental Quantification of the Fractionation of Fe Isotopes during Metal Segregation from a Silicate Melt. *Earth Planet. Sci. Lett.* **2006**, 248, 851–867.
- (49) Richter, F. M.; Watson, E. B.; Mendybaev, R. A.; Teng, F.-Z.; Janney, P. E. Magnesium Isotope Fractionation in Silicate Melts by Chemical and Thermal Diffusion. *Geochim. Cosmochim. Acta* **2008**, *72*, 206–220.
- (50) Goel, G.; Zhang, L.; Lacks, D. J.; Van Orman, J. A. Isotope Fractionation by Diffusion in Silicate Melts: Insights from Molecular Dynamics Simulations. *Geochim. Cosmochim. Acta* **2012**, 93, 205–213.
- (51) Watson, H. C.; Richter, F.; Liu, A.; Huss, G. R. Iron and Nickel Isotope Fractionation by Diffusion, with Applications to Iron Meteorites. *Earth Planet. Sci. Lett.* **2016**, *451*, 159–167.
- (52) Mueller, T.; Watson, E. B.; Trail, D.; Wiedenbeck, M.; Van Orman, J.; Hauri, E. H. Diffusive Fractionation of Carbon Isotopes in γ-Fe: Experiment, Models and Implications for Early Solar System Processes. *Geochim. Cosmochim. Acta* **2014**, *127*, 57–66.
- (53) Lundstrom, C. C.; Chaussidon, M.; Hsui, A. T.; Kelemen, P.; Zimmerman, M. Observations of Li Isotopic Variations in the Trinity Ophiolite: Evidence for Isotopic Fractionation by Diffusion during Mantle Melting. *Geochim. Cosmochim. Acta* **2005**, *69*, 735–751.
- (54) Verbeek, A. A.; Schreiner, G. D. L. Variations in 39K:41K Ratio and Movement of Potassium in a Granite-Amphibolite Contact Region. *Geochim. Cosmochim. Acta* 1967, 31, 2125–2133.
- (55) Ionov, D. A.; Wang, K. Potassium Distribution and Isotope Composition in the Lithospheric Mantle in Relation to Global Earth's Reservoirs. *Geochim. Cosmochim. Acta* **2021**, *309*, 151–170.
- (56) Huang, F.; Chen, L.; Wu, Z.; Wang, W. First-Principles Calculations of Equilibrium Mg Isotope Fractionations between Garnet, Clinopyroxene, Orthopyroxene, and Olivine: Implications for Mg Isotope Thermometry. *Earth Planet. Sci. Lett.* **2013**, 367, 61–70.
- (57) Gao, C.; Cao, X.; Liu, Q.; Yang, Y.; Zhang, S.; He, Y.; Tang, M.; Liu, Y. Theoretical Calculation of Equilibrium Mg Isotope Fractionations between Minerals and Aqueous Solutions. *Chem. Geol.* **2018**, 488, 62–75.
- (58) Wang, W.; Zhou, C.; Liu, Y.; Wu, Z.; Huang, F. Equilibrium Mg Isotope Fractionation among Aqueous Mg2+, Carbonates, Brucite and Lizardite: Insights from First-Principles Molecular Dynamics Simulations. *Geochim. Cosmochim. Acta* **2019**, 250, 117–129.
- (59) Pinilla, C.; Blanchard, M.; Balan, E.; Natarajan, S. K.; Vuilleumier, R.; Mauri, F. Equilibrium Magnesium Isotope Fractionation between Aqueous Mg2+ and Carbonate Minerals: Insights from Path Integral Molecular Dynamics. *Geochim. Cosmochim. Acta* **2015**, *163*, 126–139.
- (60) Li, W.; Chakraborty, S.; Beard, B. L.; Romanek, C. S.; Johnson, C. M. Magnesium Isotope Fractionation during Precipitation of Inorganic Calcite under Laboratory Conditions. *Earth Planet. Sci. Lett.* **2012**, 333–334, 304–316.
- (61) Mavromatis, V.; Gautier, Q.; Bosc, O.; Schott, J. Kinetics of Mg Partition and Mg Stable Isotope Fractionation during Its Incorporation in Calcite. *Geochim. Cosmochim. Acta* **2013**, *114*, 188–203.
- (62) Wang, Z.; Hu, P.; Gaetani, G.; Liu, C.; Saenger, C.; Cohen, A.; Hart, S. Experimental Calibration of Mg Isotope Fractionation between Aragonite and Seawater. *Geochim. Cosmochim. Acta* **2013**, *102*, 113–123.
- (63) Teng, F.-Z. Magnesium Isotope Geochemistry. Rev. Mineral. Geochem. 2017, 82, 219–287.
- (64) Son, S.; Li, W.; Lee, J.-Y.; Kwon, K. D. On the Coordination of Mg2+ in Aragonite: Ab-Initio Absorption Spectroscopy and Isotope Fractionation Study. *Geochim. Cosmochim. Acta* **2020**, 286, 324–335.
- (65) Smith, J. V.; Anderson, A. T.; Newton, R. C.; Olsen, E. J.; Wyllie, P. J. A Petrologic Model for the Moon Based on Petrogenesis,

- Experimental Petrology, and Physical Properties. J. Geol. 1970, 78, 381-405
- (66) Wood, J. A.; Dickey, J. S., Jr.; Marvin, U. B.; Powell, B. N. Lunar Anorthosites and a Geophysical Model of the Moon. *Geochim. Cosmochim. Acta, Suppl.* **1970**, *1*, 965.
- (67) Heiken, G.; Vaniman, D.; French, B. M. Lunar Sourcebook: A User's Guide to the Moon; Cambridge University Press, 1991.
- (68) Tian, Z.; Jolliff, B. L.; Korotev, R. L.; Fegley, B.; Lodders, K.; Day, J. M. D.; Chen, H.; Wang, K. Potassium Isotopic Composition of the Moon. *Geochim. Cosmochim. Acta* **2020**, 280, 263–280.
- (69) Steele, I. M.; Hutcheon, I. D.; Smith, J. V. Ion Microprobe Analysis and Petrogenetic Interpretations of Li, Mg, Ti, K, Sr, Ba in Lunar Plagioclase. *Lunar Planet. Sci. Conf. Proc.* **1980**, *1*, 571–590.
- (70) Arai, T.; Maruyama, S. Formation of Anorthosite on the Moon through Magma Ocean Fractional Crystallization. *Geosci. Front.* **2017**, *8*, 299–308.
- (71) Hart, S. E.; Brooks, C. Clinopyroxene-Matrix Partitioning of K, Rb, Cs, Sr and Ba. *Geochim. Cosmochim. Acta* 1974, 38, 1799–1806.
- (72) Philpotts, J. A.; Schnetzler, C. C. Phenocryst-Matrix Partition Coefficients for K, Rb, Sr and Ba, with Applications to Anorthosite and Basalt Genesis. *Geochim. Cosmochim. Acta* **1970**, *34*, 307–322.
- (73) Aigner-Torres, M.; Blundy, J.; Ulmer, P.; Pettke, T. Laser Ablation ICPMS Study of Trace Element Partitioning between Plagioclase and Basaltic Melts: An Experimental Approach. *Contrib. Mineral. Petrol.* **2007**, *153*, 647–667.
- (74) Bindeman, I. N.; Davis, A. M. Trace Element Partitioning between Plagioclase and Melt: Investigation of Dopant Influence on Partition Behavior. *Geochim. Cosmochim. Acta* **2000**, *64*, 2863–2878.
- (75) Bindeman, I. N.; Davis, A. M.; Drake, M. J. Ion Microprobe Study of Plagioclase-Basalt Partition Experiments at Natural Concentration Levels of Trace Elements. *Geochim. Cosmochim. Acta* **1998**, *62*, 1175–1193.
- (76) Taylor, G. J.; Wieczorek, M. A. Lunar Bulk Chemical Composition: A Post-Gravity Recovery and Interior Laboratory Reassessment. *Philos. Trans. R. Soc., A* **2014**, *372*, 20130242.
- (77) Snyder, G. A.; Taylor, L. A.; Neal, C. R. A Chemical Model for Generating the Sources of Mare Basalts: Combined Equilibrium and Fractional Crystallization of the Lunar Magmasphere. *Geochim. Cosmochim. Acta* 1992, 56, 3809–3823.
- (78) Williams, R. J.; Jadwick, J. J. Handbook of Lunar Materials; NASA Johnson Space Center, 1980.
- (79) Warren, P. H.; Wasson, J. T. The Origin of KREEP. *Rev. Geophys.* **1979**, *17*, 73–88.
- (80) Humayun, M.; Clayton, R. N. Potassium Isotope Cosmochemistry: Genetic Implications of Volatile Element Depletion. *Geochim. Cosmochim. Acta* **1995**, *59*, 2131–2148.
- (81) Nie, N. X.; Dauphas, N. Vapor Drainage in the Protolunar Disk as the Cause for the Depletion in Volatile Elements of the Moon. *Astrophys. J.* **2019**, 884, L48.
- (82) Steiger, R. H.; Jäger, E. Subcommission on Geochronology: Convention on the Use of Decay Constants in Geo- and Cosmochronology. *Earth Planet. Sci. Lett.* **1977**, *36*, 359–362.
- (83) Faure, G. *Principles of Isotope Geology*; John Wiley and Sons, Inc.: New York, NY: United States, 1977.
- (84) Naumenko, M. O.; Mezger, K.; Nägler, T. F.; Villa, I. M. High Precision Determination of the Terrestrial 40K Abundance. *Geochim. Cosmochim. Acta* 2013, 122, 353–362.
- (85) Merrihue, C.; Turner, G. Potassium-Argon Dating by Activation with Fast Neutrons. *J. Geophys. Res.* **1966**, *71*, 2852–2857.
- (86) Criss, R. E. Principles of Stable Isotope Distribution; Oxford University Press: New York, 1999.
- (87) Young, E. D.; Galy, A.; Nagahara, H. Kinetic and Equilibrium Mass-Dependent Isotope Fractionation Laws in Nature and Their Geochemical and Cosmochemical Significance. *Geochim. Cosmochim. Acta* **2002**, *66*, 1095–1104.
- (88) Santiago Ramos, D. P.; Coogan, L. A.; Murphy, J. G.; Higgins, J. A. Low-Temperature Oceanic Crust Alteration and the Isotopic Budgets of Potassium and Magnesium in Seawater. *Earth Planet. Sci. Lett.* **2020**, *541*, 116290.

- (89) Kelley, S. K-Ar and Ar-Ar Dating. Rev. Mineral. Geochem. 2002, 47, 785–818.
- (90) Amelin, Y.; Kaltenbach, A.; Iizuka, T.; Stirling, C. H.; Ireland, T. R.; Petaev, M.; Jacobsen, S. B. U—Pb Chronology of the Solar System's Oldest Solids with Variable 238U/235U. *Earth Planet. Sci. Lett.* **2010**, 300. 343—350.
- (91) Schaen, A. J.; Jicha, B. R.; Hodges, K. V.; Vermeesch, P.; Stelten, M. E.; Mercer, C. M.; Phillips, D.; Rivera, T. A.; Jourdan, F.; Matchan, E. L.; Hemming, S. R.; Morgan, L. E.; Kelley, S. P.; Cassata, W. S.; Heizler, M. T.; Vasconcelos, P. M.; Benowitz, J. A.; Koppers, A. A. P.; Mark, D. F.; Niespolo, E. M.; Sprain, C. J.; Hames, W. E.; Kuiper, K. F.; Turrin, B. D.; Renne, P. R.; Ross, J.; Nomade, S.; Guillou, H.; Webb, L. E.; Cohen, B. A.; Calvert, A. T.; Joyce, N.; Ganerød, M.; Wijbrans, J.; Ishizuka, O.; He, H.; Ramirez, A.; Pfänder, J. A.; Lopez-Martínez, M.; Qiu, H.; Singer, B. S. Interpreting and Reporting 40Ar/39Ar Geochronologic Data. *Geol. Soc. Am. Bull.* 2020, 133, 461.
- (92) Tian, Z.; Chen, H.; Fegley, B.; Lodders, K.; Barrat, J.-A.; Day, J. M. D.; Wang, K. Potassium Isotopic Compositions of Howardite-Eucrite-Diogenite Meteorites. *Geochim. Cosmochim. Acta* **2019**, 266, 611–632.
- (93) Tian, Z.; Magna, T.; Day, J. M. D.; Mezger, K.; Scherer, E. E.; Lodders, K.; Hin, R. C.; Koefoed, P.; Bloom, H.; Wang, K. Potassium Isotope Composition of Mars Reveals a Mechanism of Planetary Volatile Retention. *Proc. Natl. Acad. Sci.* **2021**, *118*, No. e2101155118.